Lithuanian Journal of Physics, Vol. **55**, No. 1, pp. 1–9 (2015)

SOLID-STATE ^{1}H AND ^{31}P NMR AND FTIR SPECTROSCOPY STUDY OF STATIC AND DYNAMIC STRUCTURES IN SOL-GEL DERIVED CALCIUM HYDROXYAPATITES

L. Dagys [a], V. Klimavičius [a], J. Kausteklis [a], A. Chodosovskaja [b], V. Aleksa [a], A. Kareiva [b], and V. Balevičius [a]

[a] *Department of General Physics and Spectroscopy, Vilnius University, Saulėtekio 9–3, LT-10222 Vilnius, Lithuania*
[b] *Department of Inorganic Chemistry, Vilnius University, Naugarduko 24, LT-03225 Vilnius, Lithuania*
E-mail: vytautas.balevicius@ff.vu.lt

Received 22 December 2014; revised 20 January 2015; accepted 20 March 2015

Calcium hydroxyapatite containing amorphous phosphate phase (ACP-CaHA) and nano-structured hydroxyapatite (CaHA) have been prepared by two sol-gel synthesis routes. The structural organization of hydroxyl groups in both materials has been determined by means of ^{1}H MAS NMR and FTIR spectroscopy. It has been shown that the amount of structural –OH groups in nano-structured CaHA is significantly higher than that from adsorbed water and vice versa in ACP-CaHA. A precise signal shape analysis has been carried out for both studied samples. The ^{31}P NMR signals have been found being Voigt-shaped in the wide-line as well as in MAS spectra. The ^{1}H and ^{31}P spin-lattice and spin-spin relaxation time measurements have revealed that the fast spin motion takes place in ACP-CaHA. The corresponding correlation time $\tau \sim 7 \cdot 10^{-7}$ s at ~300 K has been determined. The effect of MAS rate on the ^{31}P signal shape also confirms that this motion runs in the time scale of microseconds or even nanoseconds. The magnitude of the anisotropic broadening 1220 ± 20 Hz determined for nano-structured CaHA is very close to the maximum of the dipolar ^{1}H–^{31}P coupling distribution profile estimated using CP MAS kinetics. The dynamics of ^{1}H–^{31}P spin interactions in nano-structured CaHA ($\tau \sim 3.3 \cdot 10^{-5}$ s) is much slower than in ACP-CaHA.

Keywords: solid state NMR, FTIR spectroscopy, nano-structuring, structural water, hydroxyapatites

PACS: 33.25.+k, 82.56.-b, 78.30.-j

1. Introduction

Hydroxyapatites (HA) being thermodynamically the most stable form of calcium phosphate are widely applied in implantology, orthopedic and periodontal surgery [1, 2]. Calcium hydroxyapatite ($Ca_{10}(PO_4)_6(OH)_2$, further CaHA) has been often used to study the properties of antiresorptive agents for the prevention and treatment of bone diseases [3]. Although sintered CaHA has been used as an artificial bone substitute in clinics, bone apatite is not highly crystalline hydroxyapatite. Moreover, current artificial bone substitutes are inferior to the auto-graft with respect to osteoconductivity (property to form a new bone on the surface of materials). It has been also reported that cell attachment, proliferation and differentiation behaviour is regulated on the crystallinity [4, 5]. Thus, one of the objectives of this work was to fabricate low crystalline CaHA, which is thought to show higher osteoconductivity and thus can be used as an artificial bone substitute. For these reasons two calcium hydroxyapatites containing an amorphous phosphate phase and a nano-structured one were synthesized.

Because of high sensitivity of NMR signal parameters of particular nuclei to the local environment, i. e. short-range effects, this method is well suited for the studies of very fine aspects of structural organization and dynamics in complex solids. Therefore solid-state NMR has been applied characterizing various systems containing calcium phosphates on a molecular level. ^{1}H and ^{31}P magic-angle spinning (MAS), cross-polarization (CP) kinetics, heteronuclear correlation (HETCOR), NMR relaxation time measurements have been widely exploited in these studies [6–12]. FTIR spectroscopy is also an effective tool to estimate the degree of crystallinity, content of doped ions, bulk vs. surface effects, etc. [3, 11–15]. Thus the complementary data sets can be obtained using both of these experimental techniques.

For these reasons two synthesized calcium hydroxyapatites (containing an amorphous phosphate phase and a nano-structured one) have been studied in the present work using solid-state ^{1}H and ^{31}P NMR and FTIR spectroscopy having the purposes: (i) analysis of ^{1}H MAS NMR and FTIR spectra in order to compare both synthetic HAs with respect to the structural organization of hydroxyl groups surrounding ^{31}P nuclei and to evaluate the relative contributions of static and dynamic structures in both samples; (ii) precise processing of ^{31}P MAS and wide-line NMR signal shapes by the nonlinear contour fitting using Lorentz, Gauss and Voigt functions; (iii) to study the effect of MAS rate on the ^{31}P interactions with protons in the structural hydroxyl groups and adsorbed water; (iv) ^{1}H and ^{31}P spin-lattice and spin-spin relaxation time (T_1 and T_2) measurements in order to estimate the time scale of spin motion.

2. Experiment

NMR measurements were carried out on a *Bruker* AVANCE III HD spectrometer operating at the resonance frequencies of 400 and 162 MHz for ^{1}H and ^{31}P, respectively (magnetic field of 9.4 T). All MAS (magic angle spinning) measurements were performed using a *Bruker* 4 mm H/X CP-MAS probe-head, which is capable to spin the sample up to 15 kHz rate. NMR MAS measurements were performed at the spinning rate of 5 kHz for ^{31}P and 10 kHz for ^{1}H Bloch decay (BD) experiments. The pulse sequence, which suppresses background artifacts, was employed for ^{1}H measurements. For all ^{1}H /^{31}P MAS experiments the 90° pulse length was 2.5/1.8 μs, 64/16 scans were accumulated with a repetition delay of 3/10 s, respectively. For T_1(^{1}H) measurements the saturation recovery pulse sequence with 18 variable time delays and the repetition delay between 0.5–4 s were used.

Broad band ^{31}P experiments were performed using a *Bruker* 5 mm High Power X wide-line probe-head, which allows to use high power values in a wide range of temperature (140–670 K). The spin-lattice relaxation times T_1 have been measured using a standard saturation recovery pulse sequence applying the saturation 90° pulse train containing 50 pulses. The ^{31}P 90° pulse length varied within 3–3.5 μs depending on the temperature. The signal-to-noise (S/N) ratio was sufficient for T_1(^{31}P) measurements even after 1 scan. For each T_1 measurement varying the temperature 13 variable time delays have been used. The spin-spin relaxation time T_2 has been measured using the Carr-Purcell-Meiboom-Gill (CPMG) pulse sequence. The number of variable time delays was 16 and 16 scans were accumulated with a repetition delay of 120 s.

NMR spectra were processed using the TopSpin 3.2 software. Additionally, the signal shapes were processed using the Levenberg–Marquardt method implemented in the Microcal Origin 9 and Mathcad 15 packages [16, 17].

FTIR measurements were performed at 298 K on a *Bruker* Vertex 70 spectrometer. ACP-CaHA and nano-structured CaHA (each in amount of ca 2 mg) were mixed in the ratio of 1:100 with KBr powder and pressed into a pellet using 10 tons pressing of a manually operated *Specac* hydraulic press. FTIR transmission measurements were acquired with 2 cm^{-1} spectral resolution using a globar light source and a liquid nitrogen cooled MCT detector. Total 128 interferograms were averaged and transformed into the spectrum applying the Blackman–Harris 3-Term apodization function and the zero filling factor of 2.

3. Materials

For the preparation of $Ca_{10}(PO_4)_6(OH)_2$ having different morphological features two sol-gel synthesis routes were selected. The steps and conditions are detailed in Ref. [18]. The synthesis products were characterized by scanning electron microscopy (SEM) and energy-dispersive X-ray analysis (EDX) using a Helios NanoLab 650 scanning electron microscope coupled with an energy-dispersive X-ray spectrometry system [18].

4. Results and discussion

Thanks to the proper instrumental setting high data point density measurements of ^{1}H and ^{31}P NMR spectra have been carried out for ACP-CaHA and nano-structured CaHA. Each experimental ^{1}H spectrum contains 50 points/ppm (Fig. 1), ^{31}P spectrum has 100 points/ppm (Figs. 2 and 3). Such high data point density reduces the excess degrees of freedom in the nonlinear signal contour fitting procedure targeting its flow towards the 'true' (global) minimum on the multi-parameter surface χ^2, i. e. the sum of weighted squares of deviations of the chosen theoretical model curve from the experimental points. More rigorous decision concerning the validity of the hypothetic models (signal shapes) is possible then and more fitting parameters can be used and determined unambiguously.

The most crucial factors that influence the fine details of structural organization in the products during the applied synthesis routes are not known. However, both materials can be compared with respect to the presence of structural manifolds of hydroxyl groups by means of ^{1}H NMR and FTIR spectroscopy (Fig. 1). The relative content of –OH groups can be estimated

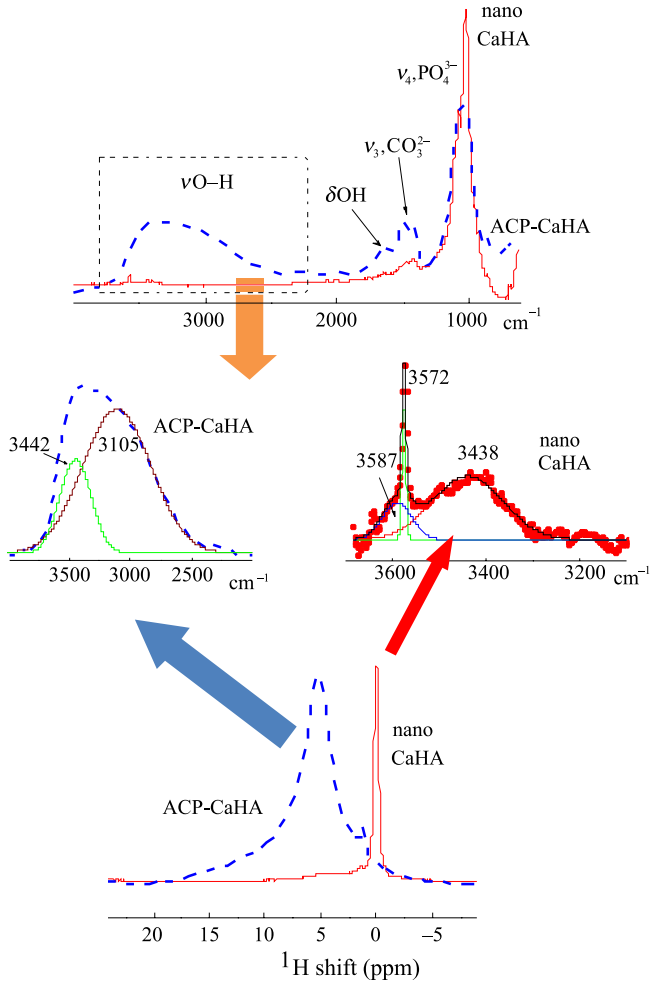

Fig. 1. The comparison of FTIR and ^{1}H MAS NMR spectra of calcium hydroxyapatite containing amorphous phosphate phase (ACP-CaHA) and nano-structured CaHA. NMR spectra are normalized to a maximum intensity. The assignments of FTIR bands follow Ref. [12].

comparing the ^{1}H MAS NMR intensities of the broad signal at ~5 ppm and the sharp peak at 0.0 ppm that are attributed to adsorbed water and structural hydroxyl groups, respectively [6, 12]. The determined ratio of integral intensities ~0.14 : 1.0 means that the amount of structural –OH groups in nano-structured CaHA is significantly higher than that from adsorbed water. As it follows from the FTIR spectra, the amount of adsorbed water in nano-structured CaHA is so low that even the band of 'free' –OH groups is seen in the spectrum (sharp peak at 3572 cm^{-1}, Fig. 1). The same feature was met in the series of FTIR spectra of Mg^{2+} and CO_3^{2-} doped hydroxyapatites [12].

The situation in ACP-CaHA looks to be an opposite. The signal at 0.0 ppm is not seen in the ^{1}H NMR spectrum and thus it can be supposed that the amount of structural hydroxyl groups is practically negligible or they are even absent. However, this can be not true. The molecules of adsorbed water possess much higher degree of motional freedom. If the amount of adsorbed water in the sample is large enough, the ^{1}H peak of the structural –OH can be significantly broadened and averaged with the water signal due to fast exchange processes. And, indeed, FTIR spectroscopy data confirm the presence of structural –OH groups in ACP-CaHA. The broad and complex-shaped νO–H contour at ~3200 cm^{-1} can be decomposed into two strongly overlapped bands with maxima at 3442 ± 2 cm^{-1} and 3105 ± 4 cm^{-1}, respectively (Fig. 1). The first one can be attributed to the stretching of structural O–H and compared with the band at 3438 ± 2 cm^{-1} in nano-structured CaHA. The second band (3105 cm^{-1}) is originated from O–H stretching of water molecules in H-bond networks [19]. The characteristic band of δOH bending vibration at 1645 cm^{-1} is also present in the FTIR spectrum. Hence the amount of adsorbed water in ACP-CaHA is high indeed. The ratio of adsorbed water and structural hydroxyl groups in ACP-CaHA can be determined using the integral intensities of the FTIR bands at 3442 and 3105 cm^{-1} and it was 3.4 : 1.0 (in comparison with the above value 0.14 : 1.0 for nano-structured CaHA).

Several minor peaks seen in the spectra of both samples at 0.5–3.0 ppm were also observed for other HAs [6, 12]. However, as noted there, their assignment is still controversial. Since these peaks do not

appear in $^{31}P \rightarrow ^{1}H$ CP MAS NMR spectra, they are most probably originated from either highly mobile or too distant to ^{31}P protons [6]. Some features in the FTIR spectra at 3587 cm^{-1}, i. e. the band much broader than 'free' OH (Fig. 1), can be related to those.

Solid-state ^{31}P NMR spectra and the signal shape analysis are often exploited in the studies of some closely related systems [8–12]. The narrow Lorentz-shaped peak at a maximum around 3 ppm and the full width at a half maximum ($\Delta\nu_{1/2}$) of 109 Hz was registered in the synthetic crystalline HA, whereas that from mesoporous bioactive glass was Gauss-shaped and an order of magnitude broader (1020 Hz) [8]. A single ^{31}P signal centered at 2.3 ppm is also displayed in fluoroapatite (FAp) gelatin nano-composite [9]. This signal was attributed to PO_4^{3-} groups in crystalline FAp. Its $\Delta\nu_{1/2}$ of 178 Hz is typical of that of pure HA and deviates significantly from that observed in HA-based nano-composite prepared by direct precipitation in a solution (373 Hz). The broadening of the latter was explained by the presence of an amorphous calcium phosphate (CaP) phase located at the surfaces or at grain boundaries of the HA nano-platelets [9]. The signal at 2.6 ppm is dominating in the ^{31}P MAS NMR spectra of CaP and gel/CaP, similarly to pure HA [10]. Therefore this peak was also attributed to PO_4^{3-} groups. However, the signal shapes in both CaP and gel/CaP are asymmetric and significantly broader, demonstrating structural inhomogeneities, which can include the presence of an additional phase difference from pure crystalline HA. The linewidths were found to increase from 243 to 373 Hz when gelatin was introduced into the mineral matrix [10]. It should be noted that for several systems decomposition of the observed ^{31}P signal into 2–3 spectral components was obtained [9–12]. These components have been attributed to bulk PO_4^{3-} (2.5–3.2 ppm), surface unprotonated PO_4^{3-} (4.4–6.0 ppm) and to protonated bulk/surface HPO_4^{2-} groups (0.45–1.3 ppm), respectively [9, 12].

A precise signal shape analysis has been carried out in the present work for both studied samples using a huge experimental dataset (>4000 points per contour). First of all, the possibility of the multiple peak fit was checked using Lorentz functions. It is demonstrated by the processing of the ^{31}P MAS NMR signal of ACP-CaHA (Fig. 2). An increase of the number of spectral components leads to the improvement of χ^2 and the correlation coefficient (R^2). However, some apparent systematic (non-random) deviations persist on the top- and wing parts of the contours (Fig. 2) despite the fact that more variable fitting parameters were included.

The ^{31}P NMR signals were found being Voigt-shaped with dominant Gauss contribution in the wide-line as well as in MAS spectra. A perfect fit

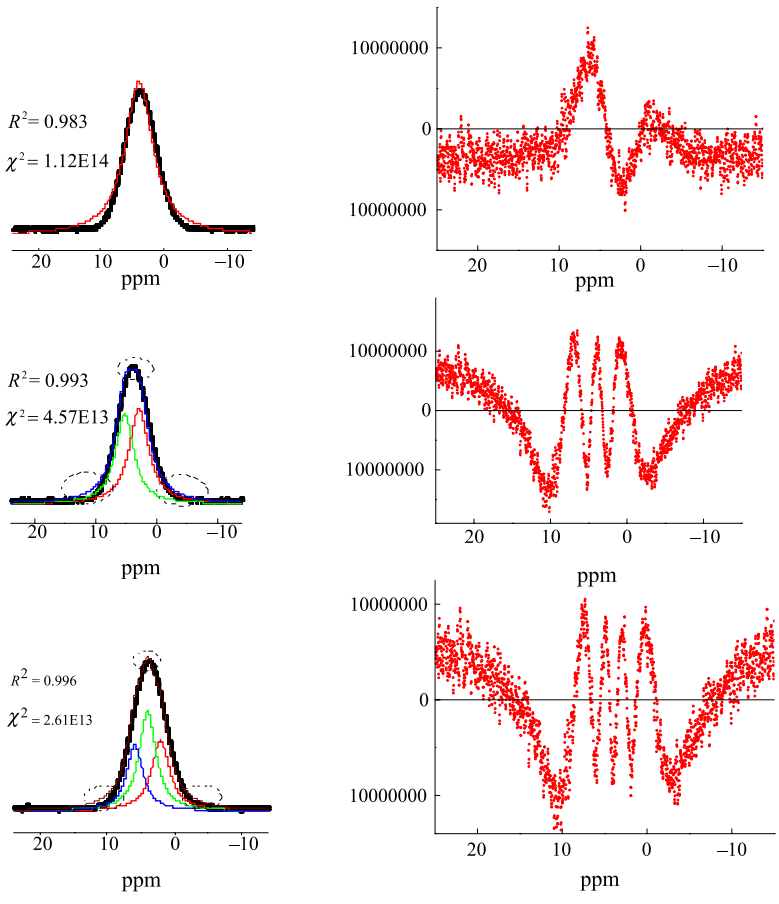

Fig. 2. The processing of the ^{31}P MAS NMR signal of ACP-CaHA using Lorentz functions: increasing the number of spectral components leads to the improvement of the fit parameters (χ^2 and R^2); however, the regions of non-random deviations survive (shown by dashed circles) despite more variable parameters included. The residuals are shown in the panels on the right.

($R^2 \cong 0.990$–0.999) was achieved using a single Voigt function for both samples (Fig. 3). The signal maxima at 3.5–3.9 ppm (MAS) and 4.7–4.8 ppm (static) get into the range of ^{31}P chemical shifts of bulk and surface PO_4^{3-} groups in the related systems reviewed above [8–12]. Much more interesting seem the signal shape and width evolution observed upon MAS.

The Voigt profile is the convolution of Gauss (G) and Lorentz (L) functions, i. e. $V = G \cdot L$. In the NMR studies of structuring effects it can be assumed that the presence of various non-uniformities (short-range disorder, heterogeneities, etc) in nano- and mesoscopic scales enhances the Gauss contribution to the Voigt-shaped signals, whereas the Lorentz contribution is originated from uniform spin interactions and dynamics. Random reorientational molecular motion can be modelled by the angular correlation function of simple exponential decay $C(t - t') \sim \exp(-k \mid t - t' \mid)$, where k is the rate constant [20, 21]. The Fourier transform of $\exp(-k \mid t - t' \mid)$ produces the Lorentz-shaped spectral profile.

The MAS technique fails to suppress anisotropic spin interactions fully if intensive reorientational dynamics is present [20, 21]. This causes different MAS effect on the ^{31}P interaction with protons in the structural hydroxyl groups and adsorbed water. The effect of MAS is indeed much less pronounced on the ^{31}P NMR spectrum of ACP-CaHA. The signal is narrowing from ~4000 Hz (static sample) to 940 Hz (MAS, at 5–10 kHz spinning, Fig. 4(a)). In the spectrum of nano-structured CaHA, which contains structural –OH/adsorbed water in the ratio 1.0/0.14 (i. e. the ratio of integrals in Fig. 1), the observed signal narrowing is very significant – from 2540 Hz (static sample) to the width 150–67 Hz that depends on the spinning rate (MAS, 1–8 kHz, Fig. 4(b)), respectively.

In the presence of reorientational motion the rotor-synchronized MAS linewidth ($\Delta\nu_{1/2}$) becomes dependent on the strength of anisotropic spin interactions, such as dipolar coupling, chemical shift anisotropy, etc (the term of the magnitude of inhomogeneous anisotropic broadening ν_{an} will be used

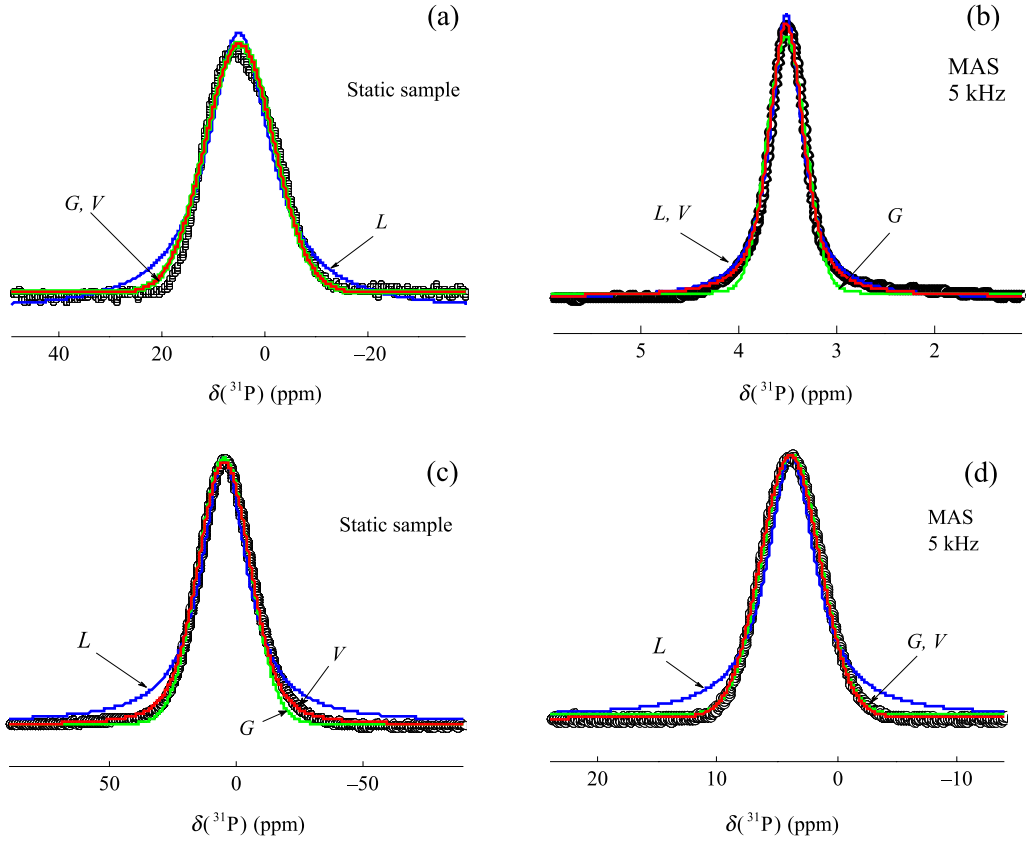

Fig. 3. The fitting of the experimental ^{31}P NMR signal contours (black) by single Voigt function (red online): nano-structured CaHA ((a) static, (b) MAS) and ACP-CaHA ((c) static, (d) MAS), respectively. The results of processing using single Gauss (green online) and Lorentz (blue online) functions are shown for comparison.

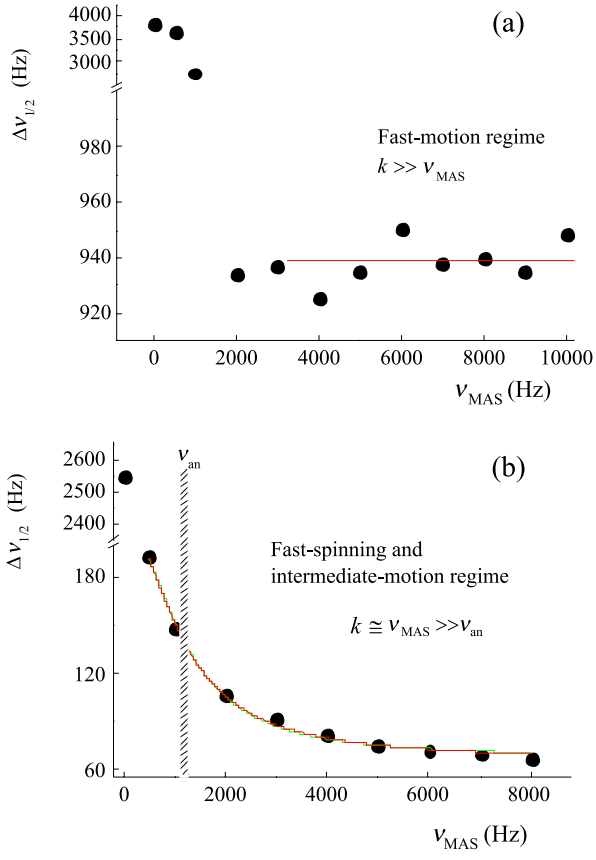

Fig. 4. Effect of the MAS rate on the ^{31}P NMR linewidth for ACP-CaHA (a) and nano-structured CaHA (b).

hereinafter), the kinetics (represented by the rate constant k) and the spinning rate (ν_{MAS}) [21]. In the fast-spinning regime the linewidth $\Delta\nu_{1/2}$ can be expressed as

$$\Delta\nu_{1/2} = \frac{\pi\nu_{an}^2}{2\nu_{MAS}(16\pi^2 + x^2)^2}$$

$$\times [-16\pi^2(e^{-x} - 1 - x) + x^2(e^{-x} - 1 + x)], \quad (1)$$

where $x = k/\nu_{MAS}$. In the regime close to the maximum broadening ($2\pi\ \nu_{MAS}/k \approx 0.55$) this equation can be simplified:

$$\Delta\nu_{1/2} = \frac{k\pi\nu_{an}^2}{2k^2 + 32\pi^2\nu_{MAS}^2}. \quad (2)$$

Both Eq. 1 and Eq. 2 have been used in processing the effect of MAS rate on the ^{31}P NMR linewidth for ACP-CaHA and nano-structured CaHA (Figs. 4 and 5). Some distinguishing features have to be noted. The signal width of the ACP-CaHA sample drops steeply down as ν_{MAS} oversteps ~1 kHz and becomes independent of the spinning rate up to 10 kHz, i. e. the maximum value used in the present work (Fig. 4(a)). This can occur if, according to Eq. 2, $k >> 4\pi\nu_{MAS}$. It means that the fast spin motion takes place in ACP-CaHA. The correlation time of this motion $\tau = k^{-1}$ gets into the time scale of microseconds or even nanoseconds. Returning to Fig. 1, which evidences that the ratio of adsorbed water and structural hydroxyl groups in ACP-CaHA was found as 3.4 : 1.0, such fast dynamics can be attributed to the rotational diffusion of adsorbed water molecules.

The situation in nano-structured CaHA is quite different. The signal width is drastically narrowed already at rather slow spinning (ν_{MAS} ~500 Hz, Fig. 4(b)). The linewidth in the MAS range 0.5–8 kHz becomes dependent on the spinning rate (Fig. 4(b)). This dependence has been processed using Eqs. 1 and 2. However, both equations are valid in the fast-spinning regime, i. e. ν_{MAS} is large compared with ν_{an} [21]. Therefore the fitting was repeated for several experimental data sets composed increasing the minimal value of the spinning rate $(\nu_{MAS})_{min}$ (Fig. 5). The values of the magnitude of the inhomogeneous anisotropic broadening

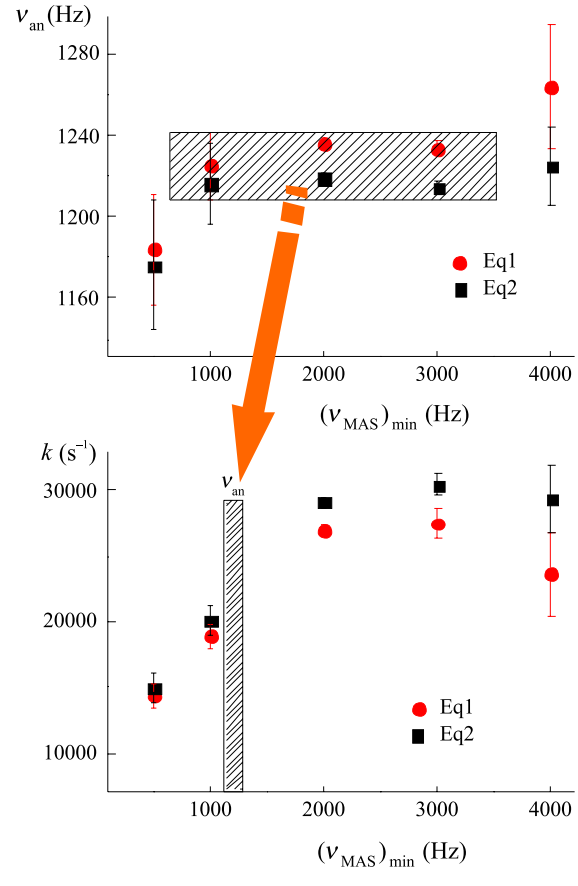

Fig. 5. Magnitude of the inhomogeneous anisotropic broadening ν_{an} and the rate constant k determined processing the experimental data sets composed by increasing the minimal value of the spinning rate $(\nu_{MAS})_{min}$ for nano-structured CaHA. More comments are given in the text.

ν_{an} as well as the rate constant k have been determined with the least errors processing the data set that starts from $(\nu_{MAS})_{min}$ = 2 kHz (Fig. 5) despite an identical coincidence between experimental points and theoretical curves (solid lines, Fig. 4(b)). Hence, the fast-spinning regime ($\nu_{MAS} > \nu_{an}$) for nano-structured CaHA is fulfilled at the spinning rates above ~2 kHz. It should be noted that the value ν_{an} = 1220 ± 20 Hz is very close to 1185 Hz that corresponds to the maximum of the dipolar ^{1}H–^{31}P coupling distribution profile in this sample determined from ^{1}H–^{31}P CP MAS kinetic experiments [18]. The rate constant k ~ 30 000 s^{-1} (Fig. 5(b)) means that the spin dynamics is much slower than in ACP-CaHA.

The measurements of ^{1}H and ^{31}P spin-lattice and spin-spin relaxation times (T_1 and T_2) have confirmed that the fast spin motion takes place in ACP-CaHA (Fig. 6). T_1 has been measured using a standard saturation recovery and T_2 has been measured using CPMG pulse sequences, respectively (see Experiment). The data have been processed using the well-known formula [22] for T_1 and T_2 for the heteronuclear dipole-dipole relaxation mechanism for spins I, S = 1/2 (spin I relaxed by spin S) that in the present case correspond to ^{31}P and ^{1}H, respectively:

$$\frac{1}{T_1} = \frac{2}{15}\overline{b^2}\{J(\omega_I - \omega_S) + 3J(\omega_I) + 6J(\omega_I + \omega_S)\}, \quad (3)$$

$$\frac{1}{T_2} = \frac{1}{15}\overline{b^2}\{4J(0) + J(\omega_I - \omega_S) + 3J(\omega_I) + 6J(\omega_S) + 6J(\omega_I + \omega_S)\}, \quad (4)$$

$$J(\omega) = \frac{\tau}{1+\omega^2\tau^2}, \quad (5)$$

$$b = -\frac{\mu_0}{4\pi}\frac{\hbar\gamma_I\gamma_S\sqrt{S(S+1)}}{r^3}, \quad (6)$$

where $J(\omega)$ is the normalized spectral density, ω_I and ω_S are the resonance (Larmor) frequencies, b is the dipole-dipole coupling constant, γ_I and γ_S are the magnetogyric ratios, r is the distance between interacting spins and τ is the rotational correlation time. In the case of spin clusters the dipole-dipole coupling constant b has to be averaged over all interacting spin pairs. A certain cluster model is then necessary. However, the rotational correlation time τ can be calculated avoiding this procedure if both T_1 and T_2 have been measured.

The measurement of T_2 for ACP-CaHA at ~300 K was performed. The rotational correlation time $\tau = 8.2 \cdot 10^{-7}$ s has been calculated considering ^{31}P–^{1}H interactions to be dominant and $\tau = 6.7 \cdot 10^{-7}$ s would follow in the case of the homonuclear ^{31}P–^{31}P coupling. Thus, the 'average' value $\tau \sim 7 \cdot 10^{-7}$ s means that the spin motion in ACP-CaHA is almost two orders faster than in nano-structured CaHA deduced from the dependence of the linewidth on the MAS rate (Fig. 5), i. e. k ~ 30 000 s^{-1}, $\tau = k^{-1} \sim 3.3 \cdot 10^{-5}$ s.

It is interesting to note very weak dependences of the relaxation time of 'fast' O–H signals on temperature as in ACP-CaHA as well as in nano-structured CaHA (Fig. 6). This observation reminds us of the behaviour of νO–H bandwidths in the FTIR spectra of propanol H-bond aggregates isolated in the cavities of argon matrix [23] and shows that the molecules of ad-

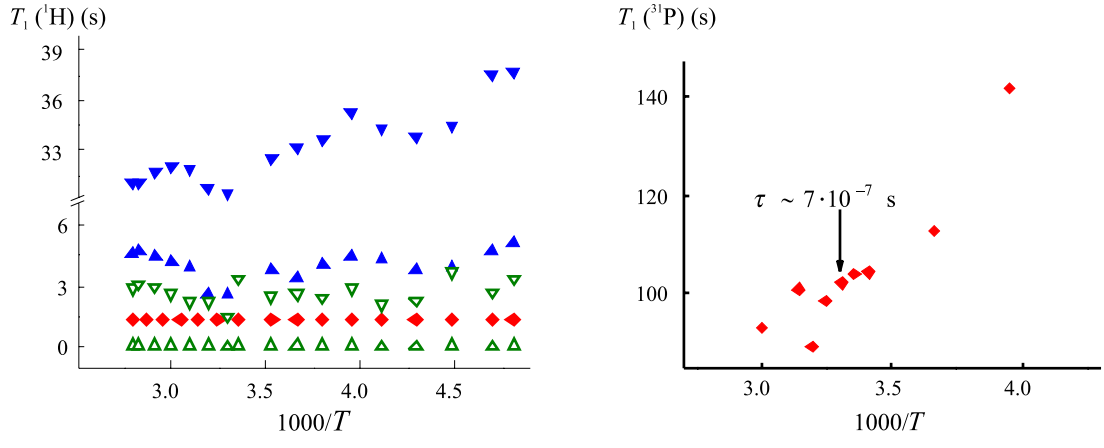

Fig. 6. Dependences of ^{1}H and ^{31}P spin-lattice relaxation time on temperature in ACP-CaHA (●) and in nano-structured CaHA (● 'fast', ■ 'slow' spectral components of structured water and ● 'fast', ■ 'slow' spectral components of adsorbed water signals, respectively; i. e. the peaks at ~0 ppm and 5 ppm (see Fig. 1)).

sorbed water can also be captured in certain studied porous materials.

5. Conclusions

1. Calcium hydroxyapatite containing amorphous phosphate phase (ACP-CaHA) and nano-structured calcium hydroxyapatites (CaHA) have been prepared by two sol-gel synthesis routes. Their structural organization with respect to hydroxyl groups has been determined by means of ^{1}H MAS NMR and FTIR spectroscopy. It has been shown that the amount of structural –OH groups in nano-structured CaHA is significantly higher than that from adsorbed water and vice versa in ACP-CaHA.

2. A precise signal shape analysis has been carried out for both studied samples using huge experimental datasets (>4000 points per contour). The ^{31}P NMR signals were found being Voigt-shaped in the static as well as in MAS spectra.

3. The magnitude of the inhomogeneous anisotropic broadening of 1220 ± 20 Hz determined for nano-structured CaHA is very close to 1185 Hz that corresponds to the maximum of the distribution profile of dipolar ^{1}H–^{31}P coupling. The spin coupling of ^{31}P with protons in structural –OH groups can be considered the major contribution to anisotropic interactions in nano-structured CaHA. However, the dynamics of the interactions is much slower than that in ACP-CaHA.

4. The effect of MAS rate on the measurements of ^{31}P signal width and ^{1}H and ^{31}P spin-lattice and spin-spin relaxation times confirm that the fast spin motion takes place in ACP-CaHA: the corresponding correlation time $\tau \sim 7 \cdot 10^{-7}$ s at room temperature is almost two orders faster than that in nano-structured CaHA deduced from the dependence of the linewidth on the MAS rate ($\tau \sim 3.3 \cdot 10^{-5}$ s). Such fast dynamics can be attributed to the rotational diffusion of adsorbed water molecules.

Acknowledgements

Funding from the European Social Fund under Grant Agreement No. VP1-3.1-ŠMM-08-K-01-004/KS-120000-1756 is acknowledged. Postdoctoral fellowship of A.C. is funded by the European Union Structural Funds Project "Postdoctoral Fellowship Implementation in Lithuania" (No SF-PD-2012-12-31-0397).

References

[1] R.Z. Le Geros and J.P. Le Geros, Hydroxyapatite, in: *Bioceramics and Their Clinical Applications*, ed. T. Kokubo (Woodhead Publishing, Cambridge, 2008) pp. 367–394.

[2] R.Z. Le Geros, *Calcium Phosphates in Oral Biology and Medicine* (Karger, Basel, 1991).

[3] P. Pascaud, P. Gras, Y. Coppel, C. Rey, and S. Sarda, Interaction between a bisphosphonate, tiludronate, and biomimetic nanocrystalline apatites, Langmuir **29**, 2224–2232 (2013).

[4] M. Kawashita, K. Taninai, Z. Li, K. Ishikawa, and Y. Yoshida, Preparation of low-crystalline apatite nanoparticles and their coating onto quartz substrates, J. Mater. Sci. Mater. Med. **23**, 1355–1362 (2012).

[5] K. Sunouchi, K. Tsuru, M. Maruta, G. Kawachi, S. Matsuya, Y. Terada, and K. Ishikawa, Fabrication of solid and hollow carbonate apatite microspheres as bone substitutes using calcite microspheres as a precursor, Dent. Mater. J. **31**, 549–557 (2012).

[6] J. Kolmas and W. Kolodziejski, Inverse ^{31}P→^{1}H NMR Cross-Polarization in hydrated nanocrystalline calcium hydroxyapatite, Chem. Phys. Lett. **554**, 128–132 (2012).

[7] W. Kolodziejski and J. Klinowski, Kinetics of cross-polarization in solid-state NMR: a guide for chemists, Chem. Rev. **102**, 613–628 (2002).

[8] R. Mathew, P.N. Gunawidjaja, I. Izquierdo-Barba, K. Jansson, A. Garcia, D. Arcos, M. Vallet-Regi, and M. Eden, Solid-state ^{31}P and ^{1}H NMR investigations of amorphous and crystalline calcium phosphates grown biomimetically from a mesoporous bioactive glass, J. Phys. Chem. C **115**, 20572–20582 (2011).

[9] A. Vyalikh, P. Simon, E. Rosseeva, J. Buder, R. Kniep, and U. Scheler, Intergrowth and interfacial structure of biomimetic fluorapatite-gelatin nanocomposite: a solid-state NMR study, J. Phys. Chem. B **118**, 724–730 (2014).

[10] A. Vyalikh, P. Simon, T. Kollmann, R. Kniep, and U. Scheler, Local environment in biomimetic hydroxyapatite-gelatin nanocomposites as probed by NMR spectroscopy, J. Phys. Chem. C **115**, 1513–1519 (2011).

[11] S. Hayakawa, T. Kanaya, K. Tsuru, Y. Shirosaki, A. Osaka, E. Fujii, K. Kawabata, G. Gasqueres, C. Bonhomme, F. Babonneau, C. Jäger, and H.J. Kleebe, Heterogeneous structure and *in vitro* degradation behavior of wet-chemically derived nanocrystalline silicon-containing hydroxyapatite particles, Acta Biomater. **9**, 4856–4867 (2013).

[12] J. Kolmas, A. Jaklewicz, A. Zima, M. Bućko, Z. Paszkiewicz, J. Lis, A. Ślosarczyk, and W. Kolodziejski, Incorporation of carbonate and magnesium ions into synthetic hydroxyapatite: the effect on physicochemical properties, J. Mol. Struct. **987**, 40–50 (2011).

[13] D. Termine and A.S. Posner, Infra-red determination of the percentage of crystallinity in apatitic calcium phosphates, Nature **211**, 268–270 (1966).

[14] T. Ishikawa, A. Teramachi, H. Tanaka, A. Yasukawa, and K. Kandori, Fourier transform infrared spectroscopy study of deuteration of calcium hydroxyapatite particles, Langmuir **16**, 10221–10226 (2000).
[15] Z.H. Cheng, A. Yasukawa, K. Kandori, and T. Ishikawa, FTIR study on incorporation of CO_2 into calcium hydroxyapatite, J. Chem. Soc. Faraday Trans. **94**, 1501–1505 (1998).
[16] *OriginLab Corporation*, http://www.OriginLab.com
[17] http://www.ptc.com/product/mathcad/
[18] V. Klimavicius, A. Kareiva, and V. Balevicius, Solid-state NMR study of hydroxyapatite containing amorphous phosphate phase and nano-structured hydroxyapatite: cut-off averaging of CP MAS kinetics and size profiles of spin clusters, J. Phys. Chem. C **118**, 28914–28921 (2014).
[19] K. Ohno, M. Okimura, N. Akai, and Y. Katsumoto, The effect of cooperative hydrogen bonding on the OH stretching-band shift for water clusters studied by matrix-isolation infrared spectroscopy and density functional theory, Phys. Chem. Chem. Phys. **7**, 3005–3014 (2005).
[20] M.M. Maricq and J.S. Waugh, NMR in rotating solids, J. Chem. Phys. **70**, 3300–3316 (1979).
[21] M.J. Thrippleton, M. Cutajar, and S. Wimperis, Magic angle spinning (MAS) NMR linewidths in the presence of solid-state dynamics, Chem. Phys. Lett. **452**, 233–238 (2008).
[22] V.I. Bakhmutov, *Solid State NMR in Materials Science* (CRC Press, Boca Raton, 2012).
[23] I. Doroshenko, V. Balevicius, V. Sablinskas, K. Aidas, G. Pitsevich, and V. Pogorelov, FTIR/PCA study of propanol in argon matrix: the initial stage of clustering and conformational transitions, Low Temp. Phys. **40**, 1384–1390 (2014).

STATINIŲ IR DINAMINIŲ STRUKTŪRŲ ZOLIŲ IR GELIŲ BŪDU SUSINTETINTUOSE KALCIO HIDROKSIAPATITUOSE TYRIMAS KIETOJO KŪNO ^{1}H IR ^{31}P BMR BEI FTIR SPEKTROMETRIJOS METODAIS

L. Dagys [a], V. Klimavičius [a], J. Kausteklis [a], A. Chodosovskaja [b], V. Aleksa [a], A. Kareiva [b], V. Balevičius [a]

[a] *Vilniaus universiteto Bendrosios fizikos ir spektroskopijos katedra, Vilnius, Lietuva*
[b] *Vilniaus universiteto Neorganinės chemijos katedra, Vilnius, Lietuva*

Santrauka

Kalcio hidroksiapatitas, savyje turintis amorfinio fosfato fazę (ACP-CaHA), ir nano- struktūrizuotas CaHA buvo pagaminti tyrimams taikant zolių ir gelių sintezės būdą. Struktūriniai abiejų junginių hidroksilo grupių organizavimosi savitumai nustatyti ^{1}H MAS ('magiško kampo sukimo') BMR ir FTIR spektrometrijos metodais. Parodyta, kad nanostruktūrizuotame CaHA, priešingai nei ACP-CaHA, struktūriškai junginio karkase priristų –OH dalis yra žymiai didesnė už hidroksilo grupių iš adsorbuoto vandens. Atlikta preciziška abiejų bandinių BMR signalų kontūrų formos analizė (>4000 taškų kontūras). Nustatyta, kad ^{31}P BMR spektrų, tiek plačiajuosčių, tiek MAS, signalų kontūrams yra būdinga Voigto forma. Tai reiškia, kad tiriamuosiuose junginiuose yra keli dinaminiai vyksmai, jų indėliai į spektrinius kontūrus aprašomi Lorentzo ir Gausso funkcijomis, o tų vyksmų spartos gali labai skirtis. ^{1}H ir ^{31}P sukinio ir gardelės bei sukinių relaksacijų trukmių (T_1 ir T_2) matavimai atskleidė ACP-CaHa junginyje labai sparčius sukinių judesius. Nustatyta judesių kambario temperatūros artumoje (~300 K) koreliacijos trukmė yra $\tau \sim 7 \cdot 10^{-7}$ s eilės. Kintamo MAS dažnio poveikis ^{31}P signalo formai taip pat patvirtina, kad ACP-CaHa junginyje vykstančių judesių laiko mastelis patenka į mikro- ar net nanosekundžių skalės sritį. Nanostruktūrizuoto CaHA nevienalyčio anizotropinio signalo išplitimo mastas 1220 ± 20 Hz puikiai dera su 1185 Hz verte, atitinkančia ^{1}H–^{31}P sukinių sąveikos skirstinio maksimumą, jis buvo nustatytas šiam bandiniui, remiantis CP ('kryžminės poliarizacijos') MAS kinetikos duomenimis. ^{1}H–^{31}P sukinių sąveikos dinamika nanostruktūrizuotame CaHA yra žymiai lėtesnė ($\tau \sim 3.3 \cdot 10^{-5}$ s) nei ACP-CaHA.